ICAS 2021 SHANGHAI
International Council of the Aeronautical Sciences
32nd Congress of the International Council of the Aeronautical Sciences
September 6-10, 2021
Pudong Shangri-La, Shanghai, China

NUMERICAL SIMULATION OF THREE-DIMENSIONAL DISTURBANCES EVOLUTION IN SUPERSONIC FLOW OVER A WAVY SURFACE

Andrey Novikov[1,2] & Alexander Fedorov[2]

[1]Central Aerohydrodynamic Institute (TsAGI), Zhukovsky, 140180, Russia
[2]Moscow Institute of Physics and Technology (MIPT), Dolgoprudny, 141701, Russia

Abstract

The stability of a near-wall flow over a grooved wavy plate in the free stream of Mach = 6 is investigated by means of spatial numerical simulations. The wavy wall produces a stabilizing effect on high-speed boundary layer by reducing second-mode instability growth that may eventually delay the laminar-turbulent transition. In this work, evolution of artificially excited three-dimensional disturbances is modeled. The Navier – Stokes equations for unsteady compressible flows of viscous perfect gas are solved using the in-house code that implements an implicit finite-volume shock-capturing method. It is shown that the wavy surface does reduce amplitudes of high-frequency plane waves, but does not dump lower frequency oblique waves. Results of three-dimensional and two-dimensional simulations are compared. This study may help to clarify robustness of wavy wall stabilization concept at high speeds.

Keywords: laminar flow control, wavy wall, high-speed boundary layer, numerical simulation

1. Introduction

To avoid early laminar-turbulent transition in high-speed boundary layer, passive laminar flow control (LFC) techniques are of primary interest. Active and reactive techniques are difficult to utilize because of severe environmental conditions of a high-speed flight associated with large heat fluxes and high temperatures of the boundary-layer flow. Passive LFC concepts include a wall shaping in meso and micro scales like ultrasonically absorptive coatings (UAC) [1] and more recent wavy wall stabilization (WWS) concept [2, 3]. Both address the second-mode dominated laminar-turbulent transition process, which naturally occurs in high-speed boundary layers.

The wavy wall stabilization concept was proposed by the authors and was confirmed by our two-dimensional (2D) numerical simulations [2] and wind-tunnel experiments [3] at free stream Mach number 6. It was shown that a specially designed wavy surface maintains a mixing layer bridging the neighboring cavities with gentle separations and reattachments on the groove tops. Because the free shear layer is more stable than the boundary layer, the wavy wall reduces the high frequency second-mode disturbance growth and, ultimately, may increase the laminar run. The effect is studied also in the works of other authors [4, 5, 6, 7] as well as by our team [8]. However, the influence of wavy-wall on three-dimensional (3D) disturbances remained unclear.

In this work, we study the WWS concept using 3D direct numerical simulations (DNS). The Navier – Stokes equations for unsteady compressible 3D flows of viscous perfect gas are solved with the in-house code. The process of laminar-turbulent transition at the supersonic freestream Mach number is initiated by artificial periodic forcing of suction–blowing type through a small hole on the wall. Modeled is an evolution of excited 3D wave-trains of different frequencies through the near-wall flow. Features of instability development over the wavy wall are explored using visualizations of the 3D disturbances field.

2. Problem formulation

2.1 Governing equations and numerical method

The equations to be solved are the three-dimensional Navier – Stokes equations in conservative dimensionless form. The fluid is a perfect gas with the specific heats ratio $\gamma = 1.4$ and Prandtl number

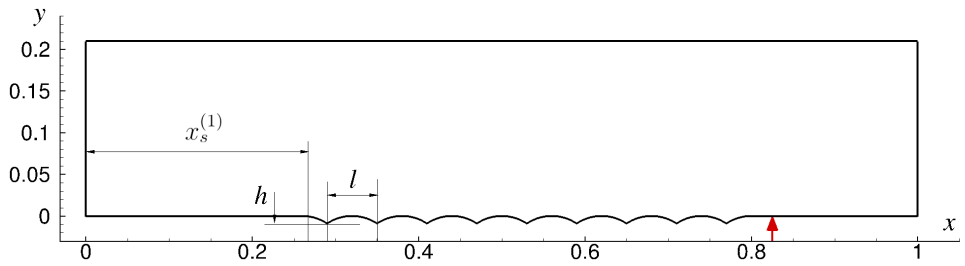

Figure 1 – Scheme of the wavy plate and computation domain in (x,y) plane. The red arrow denotes observation location $x = 0.825$.

$Pr = 0.72$. The dynamic viscosity is calculated using Sutherland's law $\mu = T^{3/2}(T_S+1)/(T_S+T)$, where $T_S = 110\,\mathrm{K}/T_\infty^*$. The coordinates $\{x,y,z\}$ are normalized to the reference length $L^* = 0.2\,\mathrm{m}$. The dependent variables $\{u,v,w,T\}$ are normalized to the corresponding freestream parameters, and pressure p – to the doubled dynamic pressure $\rho_\infty^* U_\infty^{*2}$. Hereafter asterisks denote dimensional quantities. The details of the governing equations used for the DNS may be found in e.g. [9].

The Navier – Stokes equations are integrated using the in-house solver, which implements an implicit finite-volume shock-capturing method with the second-order approximation in space and time on structured multiblock grids. Godunov-type TVD scheme with Roe approximate Riemann solver is used. Reconstruction of dependent variables at grid cell boundaries is performed using WENO-3 (Weighted Essentially Non-Oscillatory) approach, which effectively gives the third-order space approximation. The system of nonlinear discrete equations is solved using the Newton iteration method. At every iteration step, the corresponding linear algebraic system is solved using the GMRes (Generalized Minimal Residual) method. The solver employs MPI technology and PETSc framework for distributed calculations. Note that this approach is universal and most efficient if the computational domain contains shock waves and other strong spatial inhomogeneities like separation zones. The details on the numerical method may be found in e.g. [9].

The problem is solved in two steps. First, a steady laminar flow field (basic flow) is computed using the time-dependent method. Then, unsteady artificial disturbances are imposed onto this steady flow solution and unsteady problem is solved.

2.2 Flow parameters and computation domain

The computations are carried out at free-stream Mach number $\mathrm{M}_\infty = 6.0$, the unit Reynolds number $\mathrm{Re}_{\infty,1} = 10.5\times10^6\,1/\mathrm{m}$, the specific heats ratio $\gamma = 1.4$, the Prandtl number $Pr = 0.72$, free-stream static temperature $T_\infty^* = 43.18\,\mathrm{K}$. The wall is isothermal with $T_w^* = 293\,\mathrm{K}$. The reference length scale is $L^* = 0.2\,\mathrm{m}$, and the corresponding Reynolds number $\mathrm{Re}_\infty = 2.10\times10^6$. These flow parameters relate to our previous 2D numerical studies and the stability experiments [3] in Transit-M shock wind tunnel at ITAM SB RAS, Novosibirsk.

The computations are carried out for the laminar flow over the grooved wavy plate with 9 cavities and sharp leading edge at zero angle of attack. The surface shape corresponds to the experimental model [3] and is shown in figure 1. Each cavity has a form of round arc defined as

$$y(x) = \sqrt{R^2 - \left(x - x_{ss}^{(i)} - \frac{l}{2}\right)^2} - R,\; R = \frac{h}{2} + \frac{l^2}{8h},\; x_s^{(i)} < x < x_e^{(i)}$$

where $l = 0.06$, $h = 0.009$. Dimensions for the first cavity are $x_{ss}^{(1)} = 0.23$, $x_s^{(1)} = 0.26$, $x_e^{(1)} = x_s^{(1)} + l/2 = 0.29$; for the second one $x_{ss}^{(2)} = x_s^{(2)} = x_e^{(1)} = 0.29$, $x_e^{(2)} = x_s^{(2)} + l = 0.35$ and so on. The whole wavy region has the range of $0.26 < x < 0.8$. The grooving depth h is approximately equal to the boundary-layer thickness δ (for the flat plate case $\delta = 0.0105$ at $x = 0.5$).

The computational domain in (x,y) plane is shown in fig. 1. It is based on a rectangular with $[0,1]\times[0,0.21]$ extents with the bottom boundary grooved. The full 3D domain is created by extruding the 2D one along the spanwise z-axis in the range $0 \le z \le 0.15$ (see fig. 3 below).

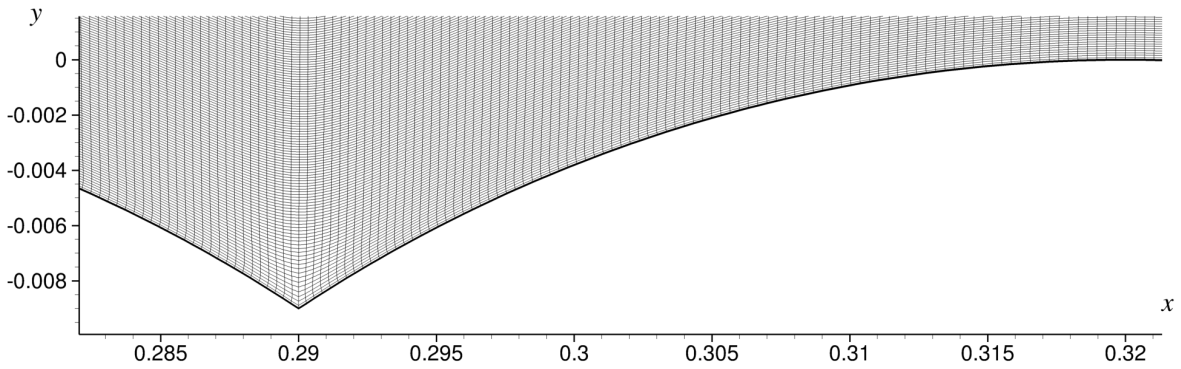

Figure 2 – Fragment of the computational grid.

In the computational domain, structured curved orthogonal grid is created with $3001 \times 401 \times 101$ nodes totaling 120×10^6 of cells. The grid have low cell skewness and fits the surface well providing wall orthogonal grid lines as seen in fig. 2. The grid nodes are clustered near the wall so that approximately 200 equidistant grid y-lines with $\Delta y = 0.84 \times 10^{-4}$ step are within the boundary layer and separation regions with the mixing layer. The spanwise grid step is $\Delta z \approx 7 \times 10^{-4}$ smoothly increasing upto $\Delta z = 35 \times 10^{-4}$ towards the $z = z_{max} = 0.15$ boundary to create a sponge zone. In the streamwise direction, the grid step is $\Delta x \approx 3 \times 10^{-4}$ that provides about 85 nodes per wavelength $\lambda = 2\pi c/\omega$ for typical second-mode disturbances with $\omega = 220$ and phase speed $c = 0.9$. For parallel calculations, the grid is splitted into $30 \times 4 \times 4$ blocks.

The time step during disturbances evolution simulation is $\Delta t = 0.0005$ that provides about 57 points per period of typical pulsation of $\omega = 220$. Computations were carried out using multiprocessor high-performance computing cluster with distributed memory. Up to 480 CPU cores were employed simultaneously for a single case.

2.3 Boundary conditions

The boundary conditions are: no-slip $u = v = w = 0$ and isothermal $T = T_w$ on the wall surface $y = y_{\min}$; the free-stream conditions $u = 1$, $v = w = 0$, $p = 1/\gamma \mathrm{M}_\infty^2$, $T = 1$ on the $x = x_{min} = 0$ (left) and $y = y_{max}$(top) boundaries; the linear extrapolation from the interior for the dependent variables u, v, w, p and T on the outflow boundary $x = x_{max}$ (right); the symmetry condition $\partial u/\partial n = \partial v/\partial n = \partial p/\partial n = \partial T/\partial n = 0$, $w = 0$ on the $z = 0$ and $z = z_{max}$ planes.

Artificial disturbances are induced via the suction-blowing like actuator modeled as the boundary condition for the vertical mass-flow perturbation

$$(\rho v)_w = \varepsilon \sin\left(\pi \frac{x - x_a + d/2}{d}\right) \sin\left(\pi \frac{z - z_a + d/2}{d}\right) \sin(\omega_a t),$$
$$x_a - \frac{d}{2} < x < x_a + \frac{d}{2}, z_a - \frac{d}{2} < z < z_a + \frac{d}{2}$$

where $x_a = 0.0625$, $z_a = 0$ and $d = 0.025$ are central point and diameter of the actuator. The actuator works continuously $0 \le t < \infty$ and generate a disturbance that transforms downstream into a spatially unstable wave train. To ensure the linear evolution of induced disturbances, a small forcing amplitude $\varepsilon = 0.001$ is chosen.

The computations are performed for several fixed angular frequencies $\omega_a = 55$, 68.75, 82.5, 110, 126.86, 142.7, 158.57, 150.64, 165, 190.28, 206.14, 220, 237.85 and 253.7. These addresses the frequency range analyzed in our previous 2D numerical simulations [3].

3. Results and discussion

The computed steady flow field over the wavy plate is shown in fig. 3. The viscous-inviscid interaction forms a bow shock in the leading-edge vicinity. The cavities induce oblique shocklets whose interaction with the boundary layer gives recirculation zones inside the cavities. The upper boundary

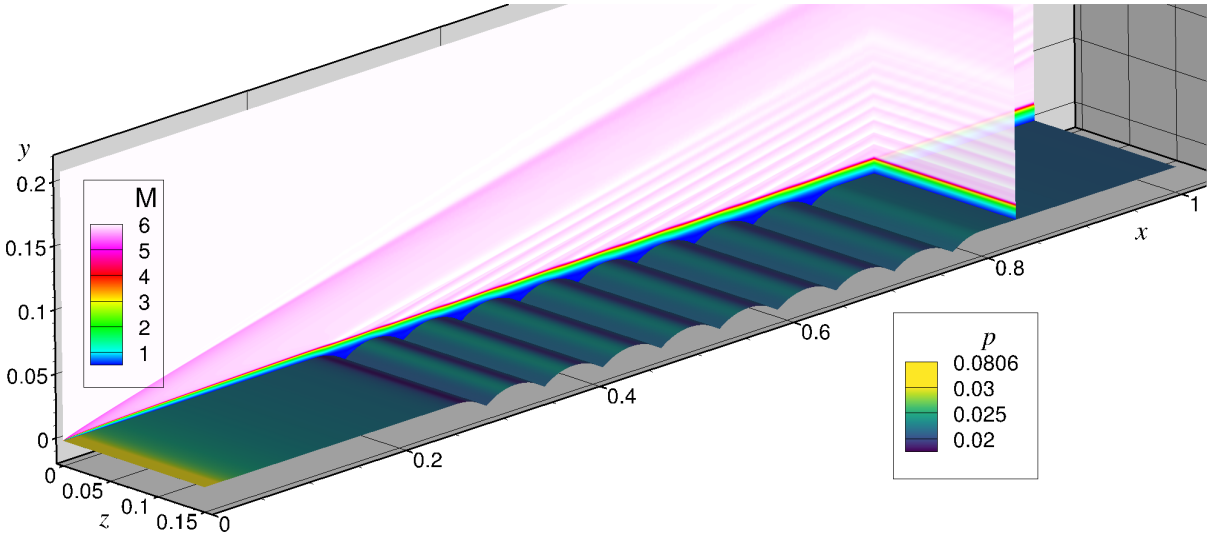

Figure 3 – Mach number field in symmetry plane and wall pressure field of the steady flow.

of each separation region is almost a straight line that gives a free shear layer bridging the cavities. This spatial steady flow pattern is almost identical to the two-dimensional one discussed in [3].

The periodic forcing imposed onto the steady boundary layer generates a wave train evolving downstream. The computed wave train for high-frequency forcing of $\omega_a = 220$ is shown in fig. 4 via instantaneous pressure disturbance field $p'(x,y,z,t)$. Hereafter, a disturbance field $f'(t)$ is obtained as the difference between a disturbed flow field and a base field $f' = f(t) - f(t=0)$.

The vortical structures of computed wave trains are shown in figures 5 and 6. These are visualized using modified Q-criterion. Normally, Q is the second invariant of the velocity gradient tensor $\nabla\{u,v,w\}$: $Q = \frac{1}{2}\left(\|\Omega\|^2 - \|\mathbf{S}\|^2\right)$, with $\Omega = \frac{1}{2}\left(\nabla V - (\nabla V)^T\right)$ and $\mathbf{S} = \frac{1}{2}\left(\nabla V + (\nabla V)^{\mathrm{T}}\right)$. In this work for clearer visualization, Q' is employed, which is the second invariant of the velocity disturbances gradient tensor $\nabla\{u',v',w'\}$.

The wall pressure pulsations amplitude $\max_t |p'_w|$ at the observation station $x = 0.825$ downstream the grooved region is shown in fig. 7 as a function of forcing frequency ω_a. The amplitude for 3D simulations is obtained by averaging over z-coordinate as

$$\left\langle p'_w(z) \right\rangle = \left[\int_{z_{min}}^{z_{max}} p'_w(z) \right] / \left[z_{max} - z_{min} \right].$$

Also shown in the figure is analogous distribution from 2D simulations [3] (the blue line) that represents spectrum of 2D waves. These distributions are normalized by their maximum values.

In high-frequency band $\omega > 200$, both distributions in fig. 7 are very close indicating that the pressure disturbance field near the wall is dominated by 2D waves. This is confirmed by the pressure disturbance footprint shown in fig. 4 for the wave train of $\omega = 220$. In the observation station $x = 0.825$, wave fronts correspond to plane waves within the wave-train core. Oblique waves, which are noticeable on the wave-train lateral sides, weakly affect the disturbance evolution. The pressure disturbance structure in the symmetry plane $z = 0$ is similar to that observed in 2D simulations [2, 8] (not shown here) and represent typical second-mode pattern. Thus, the wavy-wall effect on 3D wave trains of relatively high frequency is well captured by 2D DNS. This result is consistent with the experiment [3] showing that the wavy wall leads to significant reduction of natural disturbances in high-frequency band including the second-mode instability. Nevertheless, visualization of the vortical field using Q' criterion (see fig. 5) clearly shows the presence of 3D rope-like structures on the wave-train periphery. If these structures could trigger early nonlinear breakdown (provided that their intensity is sufficiently high) remains to be clarified.

In the low-frequency band ($\omega < 200$), 3D effect is significant: the wall-pressure amplitude of 3D wave train is larger than in the 2D case (fig. 7). This increase is most pronounced in the frequency band $140 < \omega < 160$, where the inner structure of the wave train becomes essentially 3D. As shown in

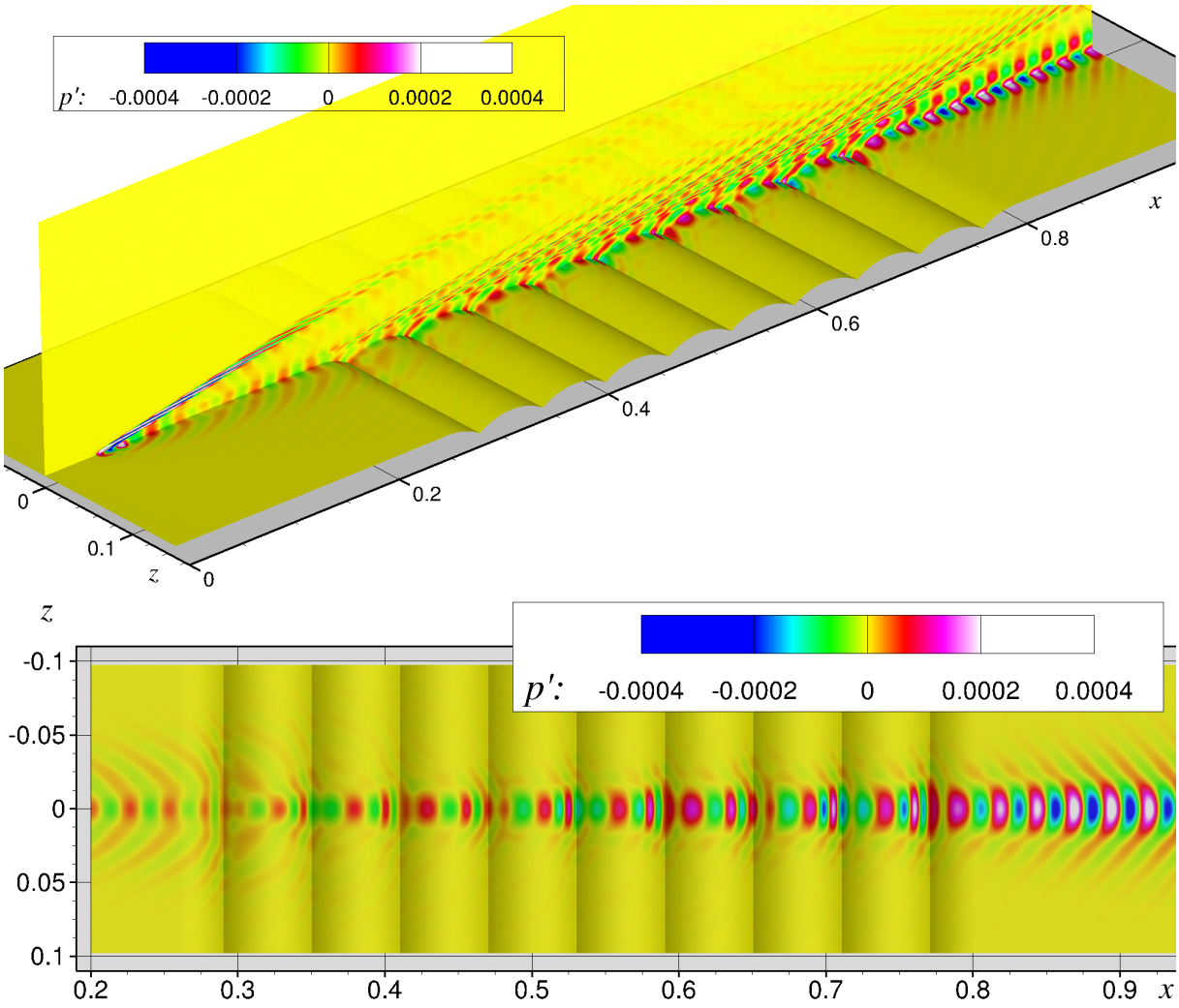

Figure 4 – The pressure disturbance field for wave train of $\omega = 220$ in symmetry plane and on the wall at time instant $t = 1.5$.

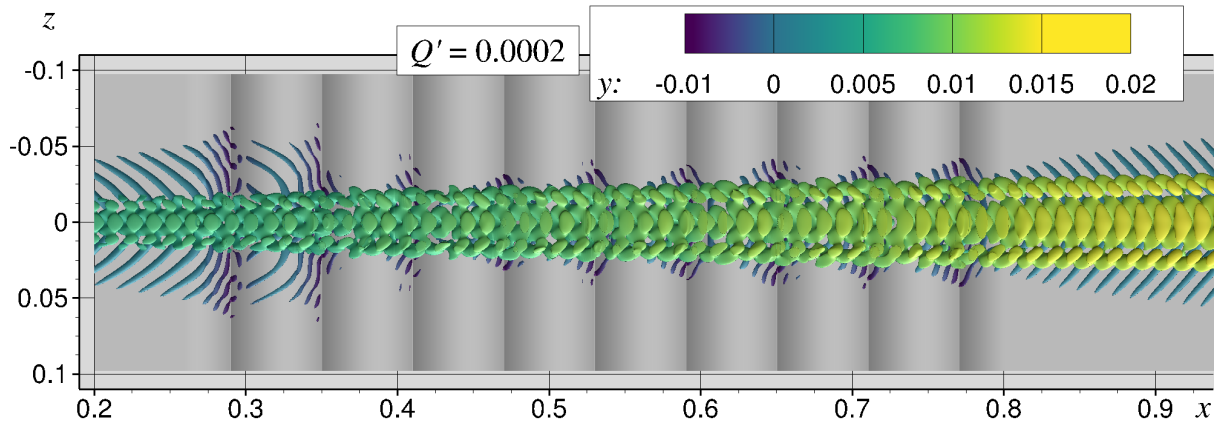

Figure 5 – Instantaneous vortical structure of the wave train of $\omega = 220$ at $t = 1.5$. Isosurface of Q' colored with the vertical distance from the wall is shown.

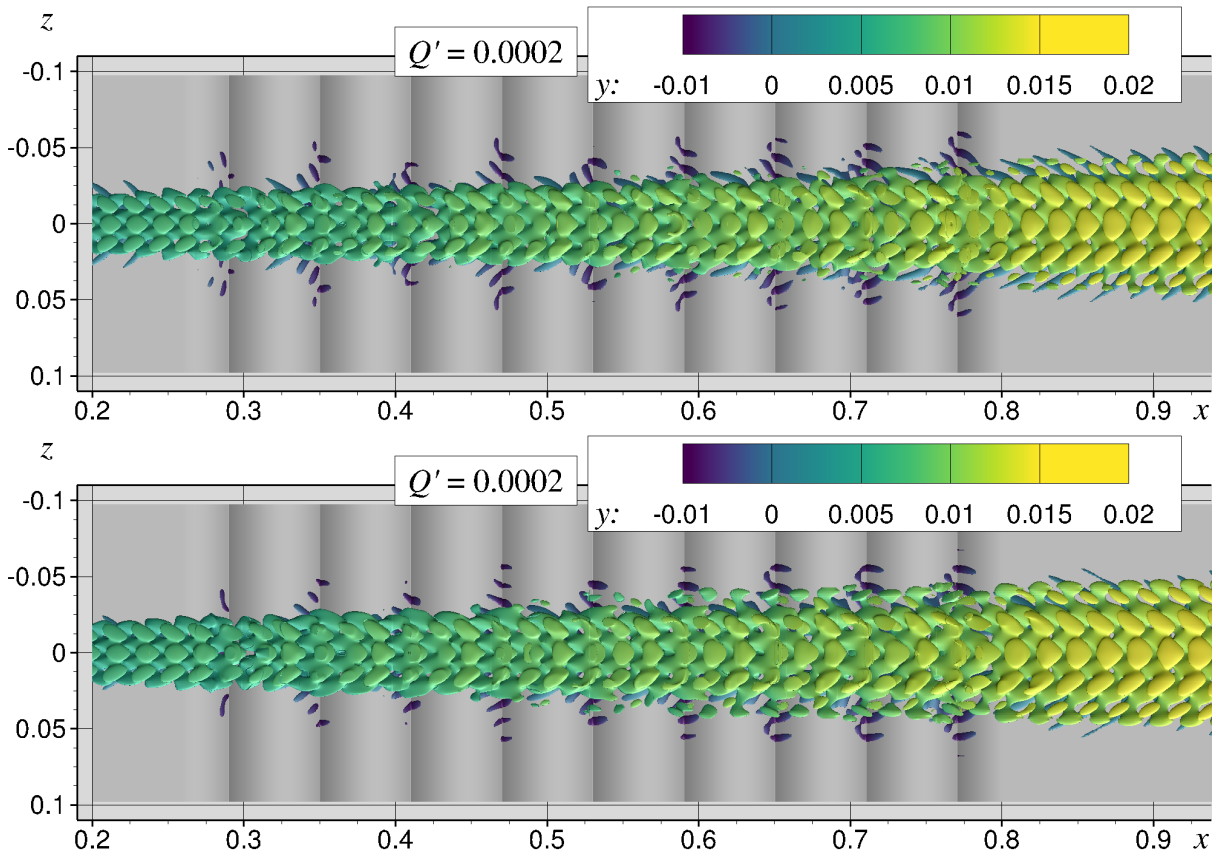

Figure 6 – Instantaneous vortical structures of the wave trains of $\omega = 158.57$ (upper) and $\omega = 142.7$ (lower) at $t = 1.5$. Isosurfaces of Q' colored with the vertical distance from the wall are shown.

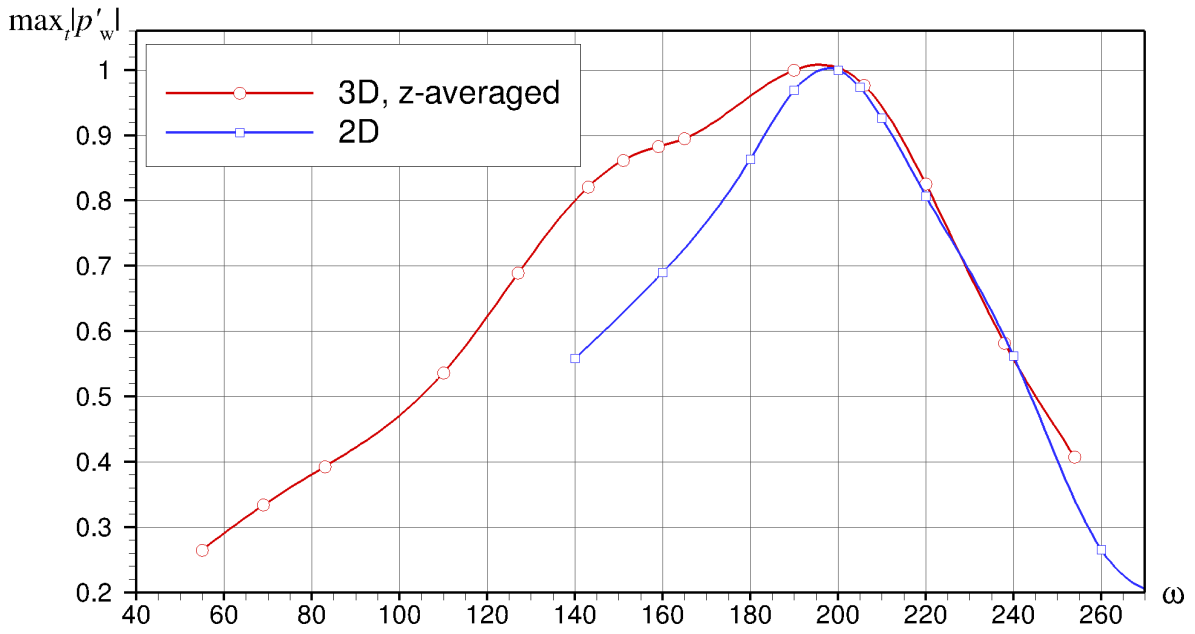

Figure 7 – The normalized wall-pressure disturbance amplitude at $x = 0.825$ for 2D waves [3] and 3D waves averaged over z-coordinate.

figure 6, the wave-train core is filled by 3D cells whose length scales in x- and z-direction are about the same. These vortical structures are observed in front of the wavy region, slowly grow propagating through it and remain dominant further downstream. They seem to be relevant to the first-mode instability.

Because the amplitude of 3D wave-trains of low frequency band $(140 < \omega < 160)$ remains lower than the maximum amplitude at $\omega = 200$ associated with wave-trains of high frequency, the wavy-wall, in general, produce a positive stabilization effect. This qualitatively agrees with the experimental results [3]. Quantitative evaluation of the wavy-wall effectiveness for stabilization of 3D disturbances and, eventually, transition delay require more numerical and experimental studies.

4. Conclusions

Stability of the supersonic near-wall flow over a grooved wavy plate is simulated by means of numerical integration of three-dimensional Navier–Stokes equations. For this purpose, modeled is evolution of 3D disturbances of different frequencies introduced into the boundary layer upstream from the wavy region by the actuator of the suction-blow type, local in space and harmonic in time. The sharp plate at zero angle of attack with the wall partially grooved with 9 cavities is considered.

It is shown that high-frequency forcing effectively excites the second mode instability in the boundary layer flow having plane 2D wave fronts. In this case, the wall pressure pulsation amplitude downstream the wavy region obtained in the present 3D computations are close to the 2D results. Thus, the wavy-wall effect on relatively high frequency disturbances may be well captured by less computationally intensive 2D numerical simulations.

It is shown that lower frequency disturbances propagating through the wavy wall cavities exhibit essentially 3D behavior with the formation of oblique rope-like structures probably relevant to the first-mode instability. In this case, the spanwise averaged amplitude of wall-pressure pulsations is larger than obtained in the 2D modeling.

In summary, the numerical simulations confirm the concept of boundary-layer stabilization with the use of a wavy wall producing a relatively stable free shear layer at sufficiently high free-stream Mach numbers. The present work provides qualitative data to clarify the feasibility of the wavy wall stabilization concept at high speeds. Quantitative evaluation of the wavy-wall effectiveness for stabilization of 3D disturbances and, eventually, transition delay require more numerical and experimental studies.

This work was supported by the Russian Scientific Foundation (project No. 19-19-00470) and has been carried out using computing resources of the federal collective usage center Complex for Simulation and Data Processing for Mega-science Facilities at NRC “Kurchatov Institute”, http://ckp.nrcki.ru/.

5. Contact Author Email Address

mailto: andrey.novikov@tsagi.ru

6. Copyright Statement

References

[1] Fedorov A.V., Malmuth N.D., Rasheed A. and Hornung H.G. Stabilization of hypersonic boundary layers by porous coatings. *AIAA J.*, Vol. 39, No. 4, 2001.

[2] Novikov A., Egorov I. and Fedorov A. Direct Numerical Simulation of Supersonic Boundary Layer Stabilization Using Grooved Wavy Surface. *48th AIAA Aerospace Sciences Meeting*, Orlando, Florida, USA, AIAA paper 2010-1245, 2010.

[3] Bountin D., Chimitov T., Maslov A, Novikov A., Egorov I., Fedorov A. and Utyuzhnikov S. Stabilization of a hypersonic boundary layer using a wavy surface. *AIAA J.*, Vol. 51, No. 5, 2013.

[4] Kirilovskiy S.V. and Poplavskaya T.V. Hypersonic Boundary Layer Stabilization by Using a Wavy Surface. *J. Phys. Conf. Ser.*, Vol. 894, p. 012040, 2017.

[5] Zhou Y., Liu W., Chai Z. and Yang X. Numerical Simulation of Wavy Surface Effect on the Stability of a Hypersonic Boundary Layer. *Acta Astronaut.*, Vol. 140, pp. 485–496, 2017.

[6] Sawaya J., Sassanis V., Yassir S., Sescu A. and Visbal M. Assessment of the Impact of Two-Dimensional Wall Deformation Shape on High-Speed Boundary-Layer Disturbances. *AIAA J.*, Vol. 56, No. 12, pp. 4787–4800, 2018.

[7] Si W., Huang G., Zhu Y., Chen S. and Lee C. Hypersonic Aerodynamic Heating over a Flared Cone with Wavy Wall. *Phys. Fluids*, Vol. 31, No. 5, p. 051702, 2019.

[8] Fedorov A.V., Novikov A.V. and Semenov N.N. Toward optimal wavy surface shape for high-speed boundary layer stabilization. *International Journal of Fluid Mechanics Research*, Vol. 47, No. 4, pp. 329–335, 2020.

[9] Egorov I.V., Novikov A.V. and Fedorov A.V. Direct numerical simulation of the laminar–turbulent transition at hypersonic flow speeds on a supercomputer. *Computational Mathematics and Mathematical Physics*, Vol. 57, No. 8, pp. 1335 -- 1359, 2017.